Journal of Chromatography A, 1217 (2010) 3876–3880

Contents lists available at ScienceDirect

Journal of Chromatography A

journal homepage: www.elsevier.com/locate/chroma

Effect of asymmetrical flow field-flow fractionation channel geometry on separation efficiency

Ji Yeon Ahn [a], Ki Hun Kim [a], Ju Yong Lee [a], P. Stephen Williams [b], Myeong Hee Moon [a,*]

[a] Department of Chemistry, Yonsei University, 262 Seongsanro, Seodaemun-gu, Seoul 120-749, South Korea
[b] Department of Biomedical Engineering, Lerner Research Institute, Cleveland Clinic, 9500 Euclid Ave, Cleveland, OH, USA

ARTICLE INFO

Article history:
Received 2 February 2010
Received in revised form 30 March 2010
Accepted 9 April 2010
Available online 2 May 2010

Keywords:
Asymmetrical flow field-flow fractionation (AF4)
FFF
Exponential channel
Uniform flow velocity
Particle separation

ABSTRACT

The separation efficiencies of three different asymmetrical flow field-flow fractionation (AF4) channel designs were evaluated using polystyrene latex standards. Channel breadth was held constant for one channel (rectangular profile), and was reduced either linearly (trapezoidal profile) or exponentially (exponential profile) along the length for the other two. The effective void volumes of the three channel types were designed to be equivalent. Theoretically, under certain flow conditions, the mean channel flow velocity of the exponential channel could be arranged to remain constant along the channel length, thereby improving separation in AF4. Particle separation obtained with the exponential channel was compared with particle separation obtained with the trapezoidal and rectangular channels. We demonstrated that at a certain flow rate condition (outflow/inflow rate = 0.2), the exponential channel design indeed provided better performance with respect to the separation of polystyrene nanoparticles in terms of reducing band broadening. While the trapezoidal channel exhibited a little poorer performance than the exponential, the strongly decreasing mean flow velocity in the rectangular channel resulted in serious band broadening, a delay in retention time, and even failure of larger particles to elute.

© 2010 Elsevier B.V. All rights reserved.

1. Introduction

Flow field-flow fractionation (F4) is a separation technique used for size fractionation of macromolecular species such as proteins, aqueous polymers, nanoparticles, cells, subcellular species, and membrane proteins, among others [1–7]. Separation in F4 is generally performed in a thin channel with a rectangular cross section by streaming a carrier liquid along the longitudinal channel axis while a secondary flow stream moves across the channel in a direction perpendicular to the channel axis. When this transverse flow or so-called crossflow is applied, sample components in the F4 channel are driven toward one wall of the channel; simultaneously, sample material is elevated from the wall by diffusion and/or by hydrodynamic lift forces. This results in vertical distribution of the sample due to the steady-state distribution near the channel wall, in which smaller particles with higher diffusion are less constrained by the crossflow force than are larger particles. The carrier liquid has a parabolic flow profile along the length of the thin channel, and smaller species therefore migrate at a higher average velocity than do larger ones. Separation is thereby achieved according to differences in hydrodynamic diameter.

The first F4 channel had a symmetric design with two permeable walls so that crossflow entered from one wall and exited through the other [8]. Later, an asymmetric channel design [9,10] in which the upper wall was replaced by a plain glass plate was adopted to simplify channel construction and to reduce the effect of uneven permeability on crossflow through the upper channel frit. This so-called asymmetrical F4 (or AF4) is currently widely utilized. A frit inlet asymmetrical flow FFF (or FI-AF4) channel was developed by incorporating a small inlet frit into the upper wall of AF4, close to the channel inlet, to enable sample injection and separation in continuous flow streams without the requirement for a separate focusing/relaxation process [11,12]. Because there is no influx of crossflow in the AF4 channel, part of the carrier liquid from the channel inlet, and the inlet frit if present, must exit through the bottom wall, which results in a gradual decrease in migration flow velocity along the channel length when the channel breadth is constant along the channel axis. The gradual decrease of flow velocity may cause an extra broadening of the eluting sample band or may result in a failure to elute in a run with high retention. Due to this limitation, a trapezoidal channel design in which channel breadth decreases linearly along the length of channel was proposed by Litzén and Wahlund [13] and has been widely utilized in numerous applications [14–19]. However, Williams [20] reported that, based on theoretical calculations, the mean channel flow velocity in an AF4 channel that decreases exponentially in breadth can remain constant throughout the channel length under certain flow condi-

* Corresponding author. Tel.: +82 2 2123 5634; fax: +82 2 364 7050.
E-mail address: mhmoon@yonsei.ac.kr (M.H. Moon).

0021-9673/$ – see front matter © 2010 Elsevier B.V. All rights reserved.
doi:10.1016/j.chroma.2010.04.021

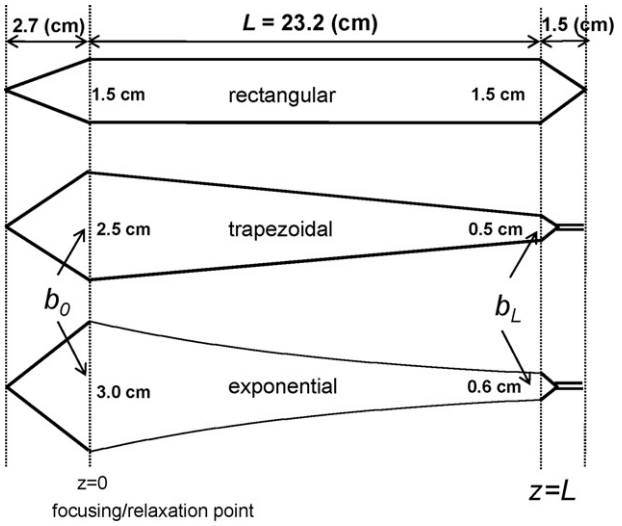

Fig. 1. Profiles of the rectangular, trapezoidal, and exponential channels with the same effective channel volume, not including the end-pieces. The ratio b_L/b_0 was 0.2 for both the trapezoidal and exponential channels.

tions, in contrast to a trapezoidal channel. This hypothesis has been theoretically validated by additional studies [21,22].

While theoretical studies have proposed that an AF4 channel with an exponential channel design can provide a constant flow velocity for the entire channel length, this hypothesis has not been confirmed experimentally. In this study, we evaluated the effect of different AF4 channel geometries on separation efficiency using submicron polystyrene (PS) latex standard mixtures. The channels had rectangular, trapezoidal, or exponential geometries, and the void volumes of the three channels were equivalent. We compared the experimental plate height values of PS particles in the different AF4 channels with or without the influence of variation in mean flow velocity depending on the channel geometry. Furthermore, we investigated the effect of different flow rate conditions in channels with different geometries by varying the flow rate conditions.

2. Theory

The AF4 channel geometries used in this study were designed to have a fixed ratio of $b_L/b_0 = 0.2$ except for the rectangular channel that had $b_L/b_0 = 1$, based on the study of Williams [20], where b_0 and b_L represent the channel breadth at the start ($z = 0$) of the channel (without considering the inlet end-piece) and at $z = L$ at the outlet, respectively, as shown in Fig. 1. In this case, L is the effective channel length along the z coordinate, w is the channel thickness, and V^0 is the effective channel void volume. In all channel cases, the starting point of sample migration as well as focusing/relaxation is $z = 0$. Likewise, the volumetric channel flowrates are $\dot{V}_0$ at $z = 0$ and $\dot{V}_L$ at $z = L$. These flow rates are slightly different from $\dot{V}_{in}$ and $\dot{V}_{out}$, respectively, in practice, because the loss of crossflow through the channel wall at both end-pieces.

The local mean carrier flow velocity, $\langle v\rangle_z$, along the channel length as a function of position z is expressed as

$$\langle v\rangle_z = \frac{\dot{V}_z}{b_z w} \tag{1}$$

where $\dot{V}_z$ and $b_z w$ represent the volumetric flow rate and the channel cross section area at any position z, respectively. Channel breadth decreases linearly from b_0 to b_L for the trapezoidal channel or exponentially for the exponential channel and can be expressed as

$$b_z = b_0 - (b_0 - b_L)\frac{z}{L} \quad \text{(for the trapezoidal channel)} \tag{2}$$

$$b_z = b_0\left(\frac{b_L}{b_0}\right)^{z/L} \quad \text{(for the exponential channel)} \tag{3}$$

$\dot{V}_z$ for each channel geometry can be expressed as a function of z, b_0, b_L and experimental parameters of $\dot{V}_0$ and $\dot{V}_L$ [20]. Likewise, b_z is a function of z, b_0 and b_L. Eq. (1) for the various channel geometries can be found in a previous publication [20]. The effective void time t^0, which is defined as the passage time of a nonretained material through the effective channel void volume, can be assumed to be the same for the three channel geometries when they are adjusted to have the same effective void volumes. The void time in this convention is calculated as follows:

$$t^0 = \int_0^L \frac{dz}{\langle v\rangle_z} = \frac{V^0}{\dot{V}_0 - \dot{V}_L}\ln\left(\frac{\dot{V}_0}{\dot{V}_L}\right) \tag{4}$$

The normalized velocity for each of the three channel geometries is expressed in [20] in such a way that local mean flow velocity $\langle v\rangle_z$ is divided by time averaged velocity $\langle\bar{v}\rangle$ as

$$\frac{\langle v\rangle_z}{\langle\bar{v}\rangle} = \ln\left(\frac{\dot{V}_0}{\dot{V}_L}\right)\left[\frac{1}{1-(\dot{V}_L/\dot{V}_0)} - \frac{z}{L}\right] \times (\text{for the rectangular channel}) \tag{5}$$

$$\frac{\langle v\rangle_z}{\langle\bar{v}\rangle} = \ln\left(\frac{\dot{V}_0}{\dot{V}_L}\right)\left[\frac{1+(b_L/b_0)}{2(1-(\dot{V}_L/\dot{V}_0))} - \frac{z}{L} + \frac{1-(b_L/b_0)}{2}\frac{z^2}{L^2}\right] \times \left(1-\left(1-\frac{b_L}{b_0}\right)\frac{z}{L}\right)^{-1} \quad \text{(for the trapezoidal channel)} \tag{6}$$

$$\frac{\langle v\rangle_z}{\langle\bar{v}\rangle} = \frac{\ln\left(\dot{V}_0/\dot{V}_L\right)}{\ln\left(b_0/b_L\right)}\left(\frac{b_0}{b_L}\right)^{z/L}\left[\frac{1-(b_L/b_0)}{1-(\dot{V}_L/\dot{V}_0)} - \left(1-\frac{b_L}{b_0}\right)^{z/L}\right] \times (\text{for the exponential channel}) \tag{7}$$

where the time averaged velocity $\langle\bar{v}\rangle$ can be calculated as L/t^0 from Eq. (4).

Because the effective channel void times for the three channel geometries are identical, the ideal retention time can be calculated from the general theory [1]

$$t_r \cong \frac{t^0}{6\lambda} \qquad \left(\lambda = \frac{l}{w} = \frac{D}{Uw}\right) \tag{8}$$

where λ is a dimensionless parameter representing the fraction of the equilibrium height l of the sample band with respect to channel thickness. In Eq. (8), D is the diffusion coefficient ($=kT/3\pi\eta d$) and U is the velocity of crossflow at the membrane ($= (\dot{V}_0 - \dot{V}_L)/A$) where kT is thermal energy, η is viscosity, d is the particle diameter, and A is the effective channel area between $z = 0$ and $z = L$. Of course, when channel void volumes and thicknesses are identical, their effective channel areas must also be identical. For a given crossflow rate, a particle would be predicted to exhibit identical λ for each of the channels. Using Eqs. (4) and (8), approximate retention time can be expressed as

$$t_r \cong \frac{\pi\eta w^2 d}{2kT}\ln\left(\frac{\dot{V}_0}{\dot{V}_L}\right) \tag{9}$$

Eq. (9) can be applied to all three channel geometries once their effective void volumes have been equalized.

Table 1
Dimensions of the three channel geometries. A_Δ is the area of the inlet end-piece (from inlet end to $z=0$), A_{eff} is the effective channel area from $z=0$ to $z=L$ ($L=23.2$ cm), and V^0_{eff} is the effective channel volume based on the measured channel thickness ($w=113$ μm).

	Rectangular	Trapezoidal	Exponential
b_0 (cm)	1.5	2.5	3.0
b_L (cm)	1.5	0.5	0.6
A_Δ (cm^2)	2.0	3.4	4.1
A_{eff} (cm^2)	34.8	34.8	34.6
V^0_{eff} (cm^3)	0.393	0.393	0.391

3. Experimental

The AF4 channels were constructed in-house using two plexiglass blocks. One block was used for the accumulation wall and had a porous frit for the crossflow passage, while the other block was used directly without insertion of a frit. The three different channel geometries were made by cutting 155-μm-thick Mylar spacers with a tip-to-tip length (L_{tt}) of 27.4 cm and an effective channel length (L) of 23.2 cm, which was fixed for all channels. Channel breadth, however, was varied as follows: the channel breadth (b) of the rectangular channel was set to 1.5 cm, and the ratios of b_L/b_0 for both the trapezoidal (0.5/2.5 cm) and exponential channels (0.6/3.0 cm) were set to be 0.2, as listed in Table 1. The channel designs are illustrated in Fig. 1. The effective channel void volumes (volume within the effective channel length L) of the three channels (rectangular, trapezoidal, and exponential geometries) were equalized to 0.39 cm^3 (the channel thickness was determined to be 113 μm in all cases). When the channel blocks were assembled, a PLCGC regenerated cellulose membrane (20 kDa MWCO) from Millipore Corp. (Billerica, MA, USA) was placed at the accumulation wall side.

Polystyrene standards with nominal diameter values of 20, 50, 93, and 135 nm were purchased from Duke Scientific Co. (Palo Alto, CA, USA). The carrier liquid used for AF4 separation was 0.05% (w/v) SDS solution to which 0.01% sodium azide was added as a bactericide. The solution was prepared using ultrapure water (>18 MΩ) and was filtered through a membrane filter with a pore size of 0.22 μm prior to use. Sample injection was performed through the channel inlet using a model 7125 loop injector with a 20 μL loop (Rheodyne, Cotati, CA, USA), while the AF4 channel was in focusing/relaxation mode. During the focusing/relaxation process, sample components achieve an equilibrium distribution above the channel wall via a balancing of the crossflow velocity and diffusion. In practice, this is achieved in such a way that the two counter-directed flow streams (one from the channel inlet and the other from the channel outlet) converge at a focusing point near the channel inlet. In our study, this was accomplished by adjusting the flow stream rates to a ratio of 1:9–1:8 so that the initial sample band was focused at $z=0$. The ratio was determined by injecting dye into the channel and visually focusing to the desired point. For PS separation, the focusing/relaxation period was set to 3 min, including sample delivery from the injector. After the focusing/relaxation period, all flows were converted to channel inlet only and the separation began. To deliver carrier liquid to the AF4 channel, a Model M930D HPLC pump from Young-Lin Co. (Seoul, Korea) was employed. Eluted PS particles were monitored with a Model 730D UV detector (cell volume: 5 μL) from Young-Lin at a wavelength of 254 nm. To provide adequate back-pressure and to regulate flow rates, a Model Whitey SS-22RS2 micrometering valve from Crawford Fitting Co. (Solon, OH, USA) was located downstream of the detector. Detector signals were recorded using Autochro-Win software from Young-Lin.

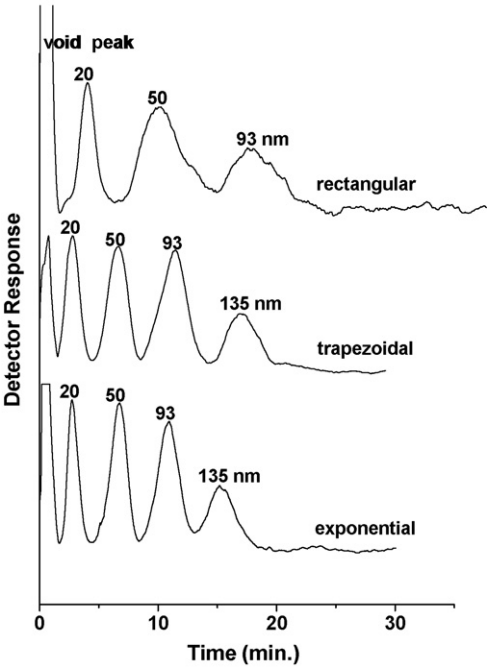

Fig. 2. Separation of PS latex standards by AF4 using different channel designs. The flow rates for the three channels were fixed at $\dot{V}_{in}/\dot{V}_{out} = 4.0/0.8$ mL/min.

4. Results and discussion

The effect of AF4 channel geometry on separation efficiency was evaluated based on the separations of polystyrene (PS) latex standard mixtures. Fig. 2 shows the separation performances of the three channel designs with identical effective void volumes using PS mixtures of 20, 50, 93, and 135 nm at $\dot{V}_{in}/\dot{V}_{out} = 4.0/0.8$ mL/min. For the rectangular channel, the PS standards eluted with relatively broad peaks with loss of 135 nm particles. The failure of the rectangular channel design to elute 135 nm PS particles under these conditions was probably due to the significant decrease in migration flow velocity along the channel axis. This is in contrast to the mean flow velocity of the trapezoidal channel, which decreased only moderately, or that of the exponential channel, which was predicted to remain approximately constant throughout the channel length under our experimental conditions. Because migration flow velocity in a rectangular channel decreases significantly along the length of the channel, the ratio of mean channel flow velocity to crossflow velocity at the membrane decreases. It is commonly found that particle standards elute with well-shaped peaks and good recovery when this ratio is maintained above some critical level. When the ratio is too low, particles tend to interact with the membrane, the retention times increase relative to predictions, and recoveries decrease. In the worst-case scenario, some particles may fail to elute. With decrease of channel breadth along the channel axis, as arranged in the trapezoidal and exponential channels, separation of the four standards was achieved. The exponential channel showed better separation performance than the trapezoidal channel. The variations in mean flow velocity along the channel axis for the three channel types, based on Eqs. (5)–(7), are plotted in Fig. 3. The solid lines in Fig. 3 represent the normalized mean flow velocity ($\langle v\rangle_z/\langle\bar{v}\rangle$) of each channel plotted along z/L for the fixed run condition of $\dot{V}_L/\dot{V}_0 = 0.2$, while the dotted lines represent the normalized mean flow velocity profiles for actual experimental flow rate conditions: $\dot{V}_L/\dot{V}_0 = 0.23$ for the rectangular channel and 0.22 for both the trapezoidal and exponential channels. The small adjustments are necessary because the

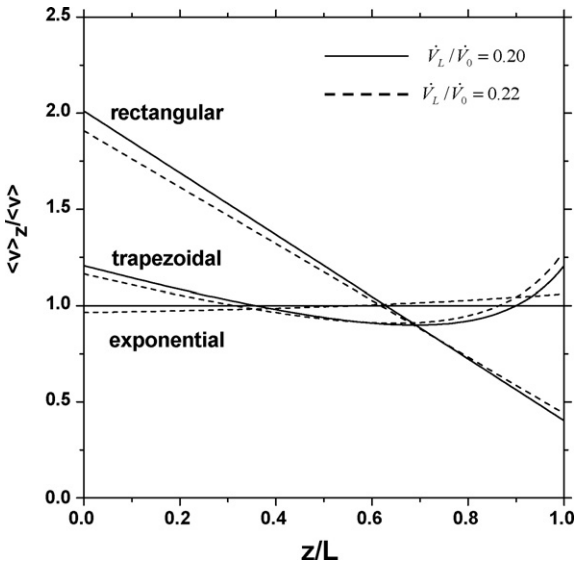

Fig. 3. Variations in the predicted velocity profiles in the three channels relative to the normalized mean channel flow velocity $\langle v\rangle_z/\langle\bar{v}\rangle$ as a function of z/L for $\dot{V}_L/\dot{V}_0 = 0.2$ (solid lines). Dotted lines represent the actual velocity profiles used in experiments: $\dot{V}_L/\dot{V}_0 = 0.23$ for the rectangular channel and 0.22 for both the trapezoidal and exponential channels.

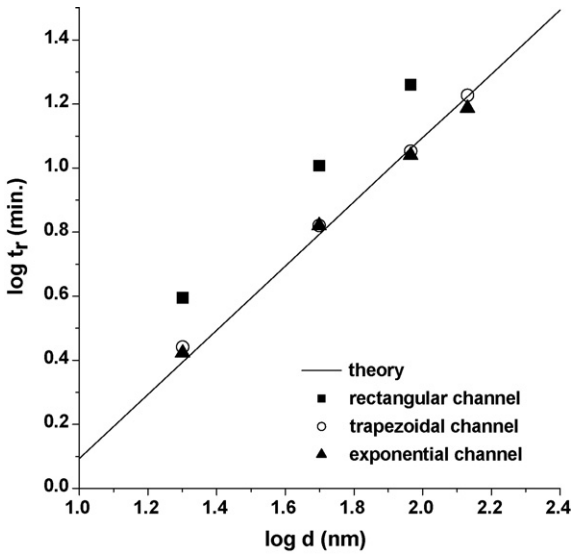

Fig. 4. Plot of the logarithm of retention time (log t_r) vs. the logarithm of particle diameter (log d) for the experimental data shown in Fig. 3. The solid line indicates the theoretical relationship.

experimental results shown in Fig. 2 were obtained at identical flow rate conditions: $\dot{V}_{in}/\dot{V}_{out} = 4.0/0.8$ mL/min. The actual $\dot{V}_L/\dot{V}_0$ values are therefore somewhat different from the optimum value of $\dot{V}_L/\dot{V}_0 = 0.2$ because a fraction of the fluid passes through the membrane within the inlet and outlet triangular end-pieces. However, the mean velocity profiles for $\dot{V}_L/\dot{V}_0 = 0.2$ and the actual profiles (for $\dot{V}_L/\dot{V}_0 = 0.22$–$0.23$) were not significantly different. As shown in Fig. 3, the normalized flow velocity decreased continuously along the channel length for the rectangular channel, while the normalized flow velocity in the trapezoidal channel showed a shallow decrease until approximately two-thirds of the channel length had been traveled, whereupon it increased rapidly. On the other hand, the exponential channel showed a slightly increasing normalized velocity along the channel length. The continuous decrease in mean velocity, as given in the rectangular channel, may result in retarded particle elution and increased band broadening.

The experimental plate height values of the PS particles measured in triplicate are listed in Table 2. Band broadening decreased as the mean velocity along the channel length approached uniformity as shown for the exponential channel. The measured plate height value of each particle size decreased from the rectangular channel design to the trapezoidal design and the exponential design, with only one exception. The 20 nm PS particles exhibited a slightly better plate height in the rectangular channel compared to the trapezoidal channel. However, this is related to the increased retention time for these particles in the rectangular channel as shown in the top fractogram in Fig. 2. While PS particles of 50 and 93 nm showed a similar increase in retention time in the rectangular channel, their peaks were much broader than those observed for the other two channels. The increased retention of the 50 and 93 nm particles in the rectangular channel may be due to increased particle–wall interaction caused by the decreasing mean fluid velocity along the channel length, and this may explain their increased plate heights. As mentioned previously, it is the increased particle–wall interaction that probably interferes with the elution of the 135 nm particles. Based on Table 2, H_{exp} of the exponential channel decreased by 20–47% compared to that of the trapezoidal channel, which indicates that uniformity of mean flow velocity along the channel length can reduce band broadening in AF4 channel systems.

Table 2
Average plate height values along with standard deviation measured in triplicate for PS standards for three different channels of AF4 at $\dot{V}_L/\dot{V}_0 = 0.23$ (rectangular) and 0.22 (trapezoidal and exponential) ($\dot{V}_{in}/\dot{V}_{out} = 4.0/0.8$ mL/min).

d (nm)	H_{exp} (cm)		
	Rectangular	Trapezoidal	Exponential
20	0.67 ± 0.18	0.79 ± 0.07	0.59 ± 0.05
50	0.75 ± 0.39	0.29 ± 0.02	0.19 ± 0.03
93	0.32 ± 0.04	0.19 ± 0.05	0.10 ± 0.01
135	–	0.14 ± 0.03	0.11 ± 0.004

Fig. 4 shows the plot of the logarithm of retention time vs. the logarithm of particle diameter for the data in Fig. 2. The solid line represents the theoretical curve based on Eq. (9) for a channel thickness value (113.0 ± 4.4 μm) that was calculated from the experimental retention time of the four PS standards obtained using the exponential channel. The difference in retention times between the trapezoidal and exponential channels shown in Fig. 4 are not significant, while the retention times of the rectangular channel show large deviations from those predicted by theory. A contribution to this large deviation may be the long passage time of particles through the triangular end-piece at the outlet; this triangular end-piece is much larger for the rectangular channel than for the other two channels (shown in Fig. 1), and the channel flow velocity is much smaller at the outlet of the rectangular channel. The presence of the large area end-piece at the outlet is geometrically unavoidable for the rectangular channel. However, this is not sufficient to fully explain the extended retention time observed for the rectangular channel.

The increase in separation efficiency observed for the exponential channel is largely attributable to the uniformity of mean flow velocity along the channel length, especially for volumetric flow rates of $\dot{V}_L/\dot{V}_0 \approx 0.2 = b_L/b_0$. Theoretical examination of mean flow velocity variations for both trapezoidal and exponential channels in an earlier study [20] suggested that an exponential channel may provide greater flexibility when selecting volumetric flow rate conditions, because this channel geometry exhibits greater mean velocity uniformity even when $\dot{V}_L/\dot{V}_0$ is not restricted to 0.2. This was examined by varying flow rate conditions for both channel designs; the separation fractograms are shown in Fig. 5.

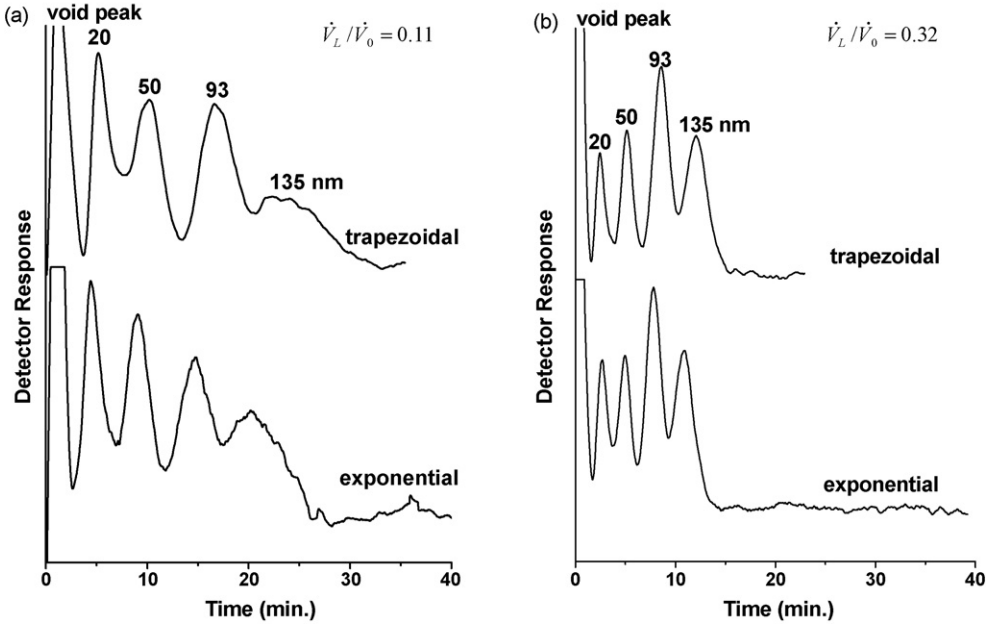

Fig. 5. Influence of $\dot{V}_L/\dot{V}_0$ on PS separation in both the trapezoidal and exponential channels. The $\dot{V}_L/\dot{V}_0$ values were (a) 0.11 and (b) 0.32. Outlet flow rates to the detector were (a) 0.4 and (b) 1.2 mL/min, and $\dot{V}_{in}$ was fixed at 4.0 mL/min for all cases.

In Fig. 5, PS separations obtained using the trapezoidal and exponential channels at flow rate conditions of (a) $\dot{V}_L/\dot{V}_0 = 0.11$ and (b) 0.32 are shown. Flow rate ratios were controlled by varying the outflow rate, $\dot{V}_{out}$ as (a) 0.4 and (b) 1.2 mL/min while fixing $\dot{V}_{in}$ at 4.0 mL/min for all runs. The values for $\dot{V}_L/\dot{V}_0$ take into account an adjustment for flow through the membrane within the triangular end-pieces. Separation of PS mixtures appeared slightly better when the exponential channel was used with $\dot{V}_L/\dot{V}_0 = 0.11$. However, the elution peak for 135 nm particles was very broad due to the influence of a stronger field strength ($\dot{V}_c = 3.6$ mL/min in Fig. 5a vs. $\dot{V}_c = 3.2$ mL/min in Fig. 2). For the case of a higher $\dot{V}_L/\dot{V}_0$, as shown in Fig. 5b, the fractograms were similar. However, peaks from the exponential channel were sharper than those from the trapezoidal channel, and there was a slight reduction in the retention time of each component when the exponential channel was used. The resolution between the peaks for 20 and 50 nm particles was slightly lower in the case of the exponential channel. Based on these experimental results, we conclude that an exponential channel separates particles better under various flow rate conditions than does a trapezoidal channel, and the use of an exponential channel can also reduce band broadening.

5. Conclusions

In this study, the effect of different AF4 channel geometries on the efficiency of separation of PS standard particles was investigated using three different channels with a rectangular, trapezoidal, or exponential geometry having an equivalent void volume. Use of a rectangular channel resulted in significant band broadening with a significant delay in retention time compared to the other two channels. This is because the mean flow velocity along the channel length of the rectangular channel decreased continuously with a large difference from the beginning to the end of the channel. Use of a trapezoidal channel reduced band broadening and removed the delay in particle retention compared to those of the rectangular channel. However, the AF4 channel with the exponential design performed better than the trapezoidal channel in terms of reducing band broadening and performing efficiently under different flow rate conditions. The exponential channel is therefore recommended for general use for AF4.

Acknowledgements

This work was supported by a grant from the Korea Research Foundation (KRF-2008-313-C00567) and in part by a grant (2009-0081904) from the Converging Research Center Program of the National Research Foundation of Korea (NRF) funded by the Ministry of Education, Science, and Technology.This paper is dedicated for the memory of Prof. Chi Sun Han.

References

[1] J.C. Giddings, Anal. Chem. 53 (1981) 1170A.
[2] J.C. Giddings, Science 260 (1993) 1456.
[3] M.E. Schimpf, K.D. Caldwell, J.C. Giddings, Field-Flow Fractionation Handbook, Wiley Interscience, New York, 2000.
[4] D. Kang, S. Oh, P. Reschiglian, M.H. Moon, Analyst 133 (2008) 505.
[5] P. Reschiglian, M.H. Moon, J. Proteomics 73 (2008) 265.
[6] D. Kang, S. Oh, S.-M. Ahn, B.-H. Lee, M.H. Moon, J. Proteome Res. 7 (2008) 3475.
[7] D. Kang, J.S. Yu, M.O. Kim, M.H. Moon, J. Proteome Res. 8 (2009) 982.
[8] J.C. Giddings, F.J. Yang, M.N. Myers, Science 193 (1976) 1244.
[9] K.-G. Wahlund, J.C. Giddings, Anal. Chem. 59 (1987) 1332.
[10] K.-G. Wahlund, A.J. Litzén, J. Chromatogr. 461 (1989) 73.
[11] M.H. Moon, H.S. Kwon, I. Park, Anal. Chem. 69 (1997) 1436.
[12] M.H. Moon, P.S. Williams, H.S. Kwon, Anal. Chem. 71 (1999) 2657.
[13] A.J. Litzén, K.-G. Wahlund, Anal. Chem. 63 (1991) 1001.
[14] B. Wittgren, K.-G. Wahlund, H. Derand, B. Wesslen, Macromolecules 29 (1996) 268.
[15] J.E.G.J. Wijinhoven, M.R. van Bommel, H. Poppe, W.Th. Kok, Chromatographia 42 (1996) 409.
[16] M. Andersson, B. Wittgren, H. Schagerlof, D. Momcilovic, K.-G. Wahlund, Biomacromolecules 5 (2004) 97.
[17] J. Luo, M. Leeman, A. Ballagi, A. Elfwing, Z. Su, J.C. Janson, K.-G. Wahlund, J. Chromatogr. A 1120 (2006) 158.
[18] E.A. Alasonati, M.A. Benincasa, V.I. Slaveykova, J. Sep. Sci. 30 (2007) 2332.
[19] D.Y. Bang, D. Shin, S. Lee, M.H. Moon, J. Chromatogr. A 1147 (2007) 200.
[20] P.S. Williams, J. Microcol. Sep. 9 (1997) 459.
[21] P. Dejardin, J. Chromatogr. A 1187 (2008) 209.
[22] P. Dejardin, J. Chromatogr. A 1203 (2008) 94.